CrystEngComm

Accepted Manuscript

ROYAL SOCIETY OF CHEMISTRY

www.rsc.org/crystengcomm

Journal Name

RSCPublishing

ARTICLE

Tracking the Transformations of Mesoporous Microspheres of Calcium Silicate Hydrate in Nanoscale upon Ibuprofen Release: An XANES and STXM Study†

Cite this: DOI: 10.1039/xoxxoooooox

Received ooth January 2012,
Accepted ooth January 2012

DOI: 10.1039/xoxxoooooox

www.rsc.org/

Xiaoxuan Guo [a], Zhiqiang Wang [a], Jin Wu [b], Yongfeng Hu [c], Jian Wang [c], Ying-Jie Zhu [b,] *, Tsun-Kong Sham [a,] *

Drug release and the accompanying biomineralization of drug carrier, mesoporous calcium silicate hydrate (CSH) microspheres, are monitored with X-ray absorption near edge structures and scanning transmission X-ray microscopy (STXM). The *in vitro* biomineralization of hydroxyapatite (HAp) on CSH microspheres is investigated by tracking specimens soaked in simulated body fluid (SBF) for various time periods; the study is complemented with X-ray powder diffraction. We clarified the presence of amorphous $CaCO_3$ at the early stage of biomineralization with solid evidences, which is still controversial from previous studies. What's more important, the observations from the STXM images and microscopy spectra directly demonstrated that amorphous SiO_2 which are from the hydrolysis of silicate ions provide the preference sites for the aggregation of HAp. These results demonstrate that XANES and STXM are sensitive techniques which can be used to analyze various bioceramics for medical applications.

Introduction

Nanostructured bioceramics nanomaterials, such as calcium phosphate ($Ca_3(PO_4)_2$, CaP) and calcium silicate (CS), have been widely applied as implants for the restoration of bone and tooth. The development of mesoporous bioceramics opens up new possibilities for drug delivery and bone therapies.[1] Since the discovery of Bioglass© by Hench and co-workers in 1971,[2] various kinds of silicates, and glasses have been investigated for hard tissue repair and replacement. Recently, CS material was proved to be excellently bioactive and a potential candidate for bone repair and therapies.[3-9] A common feature for all bioactive CS is that they can bond to living bones by forming hydroxyapatite ($Ca_{10}(PO_4)_6(OH)_2$, HAp) on their surface when they are immersed into simulated body fluid (SBF) with ion concentrations similar to human blood plasma.

In previous studies, many characterization methods have been used in the study of the transformation mechanisms from CS to HAp. Among them, X-ray diffraction (XRD), infrared spectroscopy (IR), scanning electron microscopy (SEM), transmission electron microscopy (TEM) and energy-dispersive X-ray spectrometry (EDX) are the most common techniques to study the composition, structure and morphology of the products. However, the mechanism of biomineralization of CS is still not completely clear: one controversial issue is the presence of $CaCO_3$; Siriphannon *et al.* [3] and Wan *et al.* [6] reported that $CaCO_3$ were present during the HAp formation; while Gou *et al.* [5] reported that the final products would be carbonate-containing HAp; Li *et al.* [10] reported the absence of $CaCO_3$ after the in vitro test; the other problem is about the silica-rich layer during biomineralization. Although it is well accepted that the silica-rich layer provides favorable sites for HAp precipitation, there has been no direct evidence showing the presence of silica-rich layer using the above mentioned conventional techniques.

X-ray absorption near edge structures (XANES) spectroscopy is an element specific technique, which probes the electronic states intimately associated with the absorbing atom in the vicinity of the X-ray absorption threshold (LUMO in molecules and the conduction band in semiconductor for example via dipole transitions).[11] XANES provides information on the oxidation state, coordination and symmetry of the element of interest. Materials with different structures or compositions have their unique XANES spectra at specific absorption edges (e. g.: calcium silicate hydrate (CSH), amorphous calcium phosphate, HAp and $CaCO_3$ show different XANES features at the Ca K-edge), by which qualitative analysis is very reliable by "fingerprinting".[12-16] Under favourable conditions (high quality data), quantitative information can be obtained by fitting the XANES data to a linear combination of XANES of standard components. Additionally, synchrotron source provides collimated and high photon flux that allows for

detecting the minor components (even less than 0.1 wt. % [17]) in materials no matter they are crystalline, amorphous (XRD is only suitable for crystals) or in solution. Scanning transmission X-ray microscopy (STXM)[18, 19] provides spectromicroscopic information of nanomaterials; thus both electronic and spatial features of a single nanostructure can be revealed at nanoscale (~30 nm). Therefore, the combination of STXM and XANES can monitor the spectral change and image the transformation from CSH to HAp at nanoscale simultaneously, hence affords a comprehensive understanding of the biomineralization mechanism of CSH in connection with drug release.

Previous investigations reported the formation of HAp on CS in SBF without drug loading.[3-6, 10] Few researches illustrated the bioactivity of bioactive glasses (BG) and HAp when drug were released in SBF.[20-22] Here we investigated the drug (ibuprofen, IBU) release from mesorporous CSH microspheres and the biomineralization of CSH during drug release in SBF using synchrotron based techniques (XANES and STXM). This study provides insights into the mechanism of CSH biomineralization.

Experimental

Preparation of mesoporous CSH microspheres.

CSH mesoporous microspheres were prepared by the self-assembly of CSH nanosheets via a sonochemical method.[23] 5 mL of a 4 M NaOH aqueous solution and 2 mL of tetraethyl orthosilicate (TEOS) were added into 500 mL of 0.03 M $Ca(NO_3)_2$ aqueous solution under magnetic stirring at room temperature. The resulting mixture was ultrasonically irradiated for 1 hour under ambient conditions using a high-intensity ultrasonic probe with the power of 200 W (Ti-horn, 27 kHz, Hangzhou Success, China) immersed directly in the solution. The product powder was collected after centrifugation and washed with deionised water and absolute ethanol three times, then dried in air at 60 °C overnight.

IBU drug loading.

The as-synthesized powder (1.0 g of mesoporous CSH microspheres) was added into a 50 mL IBU hexane solution (~40 mg·mL^{-1}) in a flask at room temperature. The flask was immediately sealed to prevent hexane from evaporation, and the mixture was treated by ultrasound for 2 minutes. Then the flask was oscillated at a constant rate of 160 rpm at 37 °C for 24 hours. After that the product was separated by centrifugation, washed with hexane, and dried in air at 60 °C overnight.

In vitro test.

To investigate the kinetics of IBU release from CSH microspheres and the biomineralization of CSH and to mimic those processes in the human body, experiments were carried out in a simulated body fluid (SBF). The ion concentrations of the SBF, shown in Table 1, are similar to the physiological concentrations in the human blood plasma.[24] The pH of the SBF solution was buffered at 7.40 ± 0.02 with 1 mol/L HCl and tris-(hydroxymethyl)-aminomethane [$(CH_2OH)_3CNH_2$]. 2 g of the as-synthesized CSH-IBU powder was split equally into 10 specimens (0.2 g each), and then each of them was soaked in 200 mL of SBF solution at 36.5 °C for 1, 2, 3, 4, 5, 6, 12, 24, 36, 48 hours, respectively under constant shaking (120 rpm). A portion of the IBU-release medium (2.0 mL) was extracted for UV-Vis absorption analysis (Techcomp, UV2300) at the wavelength of 263 nm at given time intervals shown above. The solid products were separated by centrifugation, rinsed with absolute ethanol, and dried in air at 60 °C overnight for XRD, SEM, TEM and XANES studies.

Table 1. Ion concentrations of SBF and human blood plasma (mmol/L)

Ion	SBF	Human Blood Plasma
Na^+	142.0	142.0
K^+	5.0	5.0
Mg^+	1.5	1.5
Ca^{2+}	2.5	2.5
Cl^-	147.8	103.8
HCO_3^{2-}	4.2	27.0
HPO_4^{2-}	1.0	1.0

Characterization.

The thermogravimetric (TG) curves were measured on a STA 409/PC simultaneous thermal analyzer (Netzsch, Germany) with a heating rate of 10 °C min^{-1} in blowing air to measure the drug loading capacities of mesoporous CSH microspheres. The morphologies of the CSH microspheres before/after IBU loading, CSH/IBU microspheres after IBU releasing in SBF for various time periods were obtained by TEM (Philips CM-10 TEM). The compositions of biomineralization products for various time periods were characterized by XRD (Rigaku D/max 2550 V, Cu Kα radiation, λ = 1.54178 Å). The concentrations of Ca, P and Si of the SBF after IBU releasing from CSH were determined using an inductively coupled plasma (ICP) instrument (JY 2000–2, Horiba, France).

XANES measurements.

XANES measurements were conducted at the Canadian Light Source (CLS) using the Soft X-ray Microcharacterization Beamline (SXRMB), which is equipped with a double crystal monochromator with two sets of interchangeable crystals operating with an energy range of 1.7 to 10 keV. The InSb (111) crystals were used for the Si K-edge XANES measurements while the Si (111) crystals were used for the Ca K-edge and P K-edge XANES. The detection modes are total electron yield (TEY) and X-ray fluorescence yield (FLY), tracking with surface and bulk sensitivities, respectively. XANES data were analyzed using the Athena XAS analysis software (http://cars9.uchicago.edu/ifeffit/Ifeffit), which is an interactive program for XAFS analysis, combining high-quality and well-tested XAFS analysis algorithms, tools for general data manipulation, and graphical display of data.

STXM measurements.

STXM measurement was conducted at the Soft X-ray Spectromicroscopy (SM) beamline at the CLS; SM is equipped with a 25 nm outermost-zone zone plate (CXRO, Berkeley Lab). The diffraction-limited spatial resolution for this zone plate is about 30 nm with a spectral resolution of 0.05 eV at the C K-edge. Image sequence (stack) scans over a range of photon energies were acquired for the same sample region at the C K-edge, Si K-edge and P K-edge. STXM data were analyzed using the aXis2000 software package (http://unicorn.chemistry.mcmaster.ca/aXis2000.html), which

allows for detailed interactive processing of the images and fitting the image stacks with the reference X-ray absorption spectra. More details about STXM measurement and data analysis can be found elsewhere.[25, 26]

Results and discussion

The morphologies of the mesoporous CSH microspheres before and after IBU loading were reported in our previous studies (Figure S1).[23, 27, 28] Figure 1 shows the micrographs of the CSH microspheres after soaking in the SBF solutions for various time periods. In comparison with the microspheres before soaking, most of the carriers remained intact after the samples were soaked in the SBF for 1 hour. At 5 hours, some microspheres were broken down; sheets-like products can be found on the edge of microspheres. After longer soaking time (24 hours and 48 hours), microspheres can be barely observed, instead, most of the microspheres turned into the aggregation of particles and flakes.

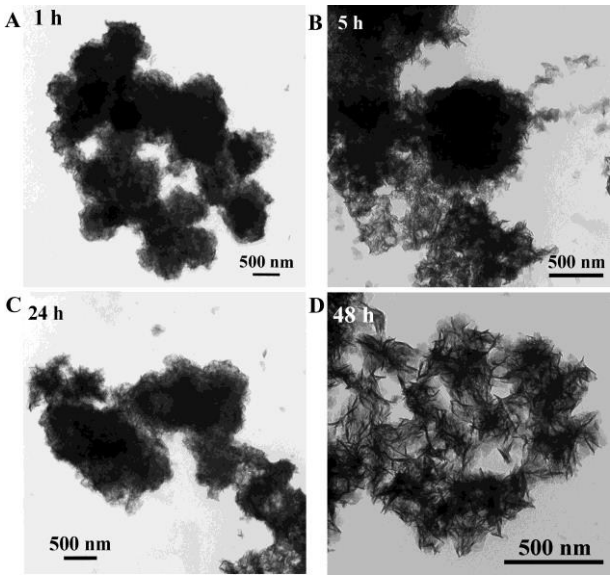

Fig. 1. TEM micrographs of CSH-IBU microspheres soaked in SBF solution for different time: (A) 1 hours, (B) 5 hours, (C) 24 hours, and (D) 48 hours.

To determine the compositions of the products having immersed in SBF solution for various period of time, XRD data of the CSH-IBU microspheres soaked in the SBF solution for various time periods were obtained as shown in Figure 2. One can see that starting from 4 h, the diffraction peaks (e.g. 2θ = 26° and 32° PDF number: 09-0432) of HAp emerge clearly in the XRD patterns. On the contrary, in the first 3 h, although weak crystalline CSH diffraction patterns can be still observed (2θ = 29° PDF number: 33-0306), a broad peak is more prominent, indicating that some amorphous components were formed, however, no further information can be revealed from XRD to illustrate the compositions of amorphous specimens.

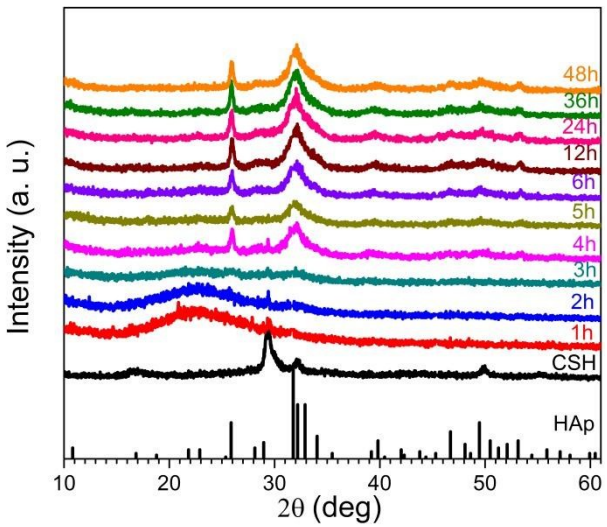

Fig. 2. XRD patterns of CSH-IBU powder soaked in SBF solution for different time.

In order to figure out the amorphous compositions of the products formed in the first several hours, XANES measurements at the Ca K-edge, P K-edge and Si K-edge were conducted (Figure 3). We only show TEY XANES for the discussions because both TEY and FLY are similar since the specimens are homogeneous and optically thin and FLY shows no detectable thickness effects. Figure 3A shows the Ca K-edge XANES of CSH-IBU microspheres after having been immersed in the SBF solution for different periods of time. There are four discernible XANES features, labelled as "a", "b", "c", and "d" as increasing photon energy. The most intense peak (feature "c") is due to Ca 1s → 4p transition. The pre-edge peak (feature "a") can be ascribed to 1s → 3d transition; the shoulder "b" is assigned to the 1s → 4s transition, both of which can be observed are due to the hybridization of Ca with ligand states of np-character, leading to the departure from perfect crystal symmetry.[29] The shoulder after the main resonance (feature "d") is mainly from multiple scattering processes.[30-32] By comparing the spectra of CSH, amorphous calcium phosphate and HAp standard samples, the main "fingerprint" differences between CSH and Hap clearly identifiable are the white line "c" and feature "d". Starting from the spectrum of 3 h (dark cyan), the spectra are almost the same as that of HAp, indicating the formation of HAp on the surface of mesoporous CSH microspheres. After a linear combination fitting procedure using standard spectra of CSH, amorphous calcium phosphate, HAp and $CaCO_3$ (Figure S2), the compositions of amorphous samples in the first 4 hours can be clearly revealed, as shown in Table 2. Combined with the results from XRD, we find that the dominant composition is amorphous HAp at the early stage of drug release, of which the percentage increase until the spectrum of 4 h which is identical to that of HAp, and it gradually becomes crystalline. Moreover, from the first several spectra, the contribution of amorphous $CaCO_3$ and calcium phosphate can also be observed, indicating that amorphous calcium phosphate was first formed then transformed into amorphous HAp rapidly, which is due to the stability of amorphous calcium phosphate in aqueous media: HAp has a lower solubility in water than other form of calcium phosphate, and $CaCO_3$ was formed during the biomineralization.

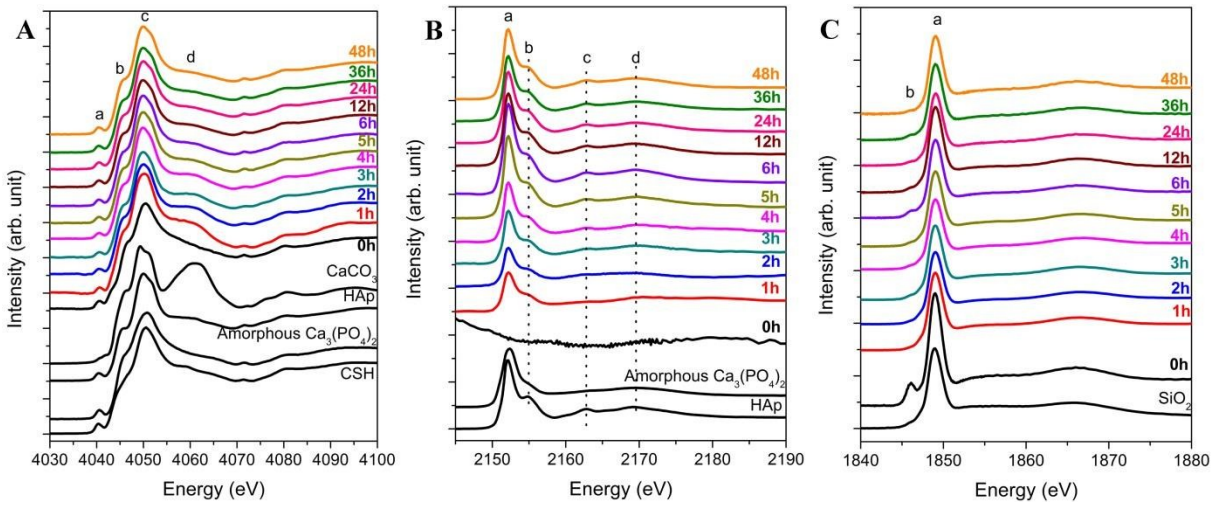

Fig. 3. Ca (A), P (B) and Si (C) K-edge XANES spectra of CSH-IBU microspheres soaked in SBF solution for various time periods.

Table 2. Ca K-edge linear combination fitting results of samples after soaked in SBF solution in the first 4 hours.

	Percentage (%)				
	CSH	$CaCO_3$	Amorphous CaP	HAp	R-factor*
1 hour	8	6	13	73	0.00298
2 hour	3	11	9	77	0.000984
3 hour	0	7	1	92	0.000809
4 hour	0	0	0	100	0.000864

* More LCF details can be found in the supporting information

The P K-edge XANES spectra also provide direct evidence for the formation of HAp. As seen in Figure 3B, there is no P signal before the samples were immersed in the SBF solution (the curve labelled as 0 h); while a strong P signal was detected after the powder was soaked in the SBF for 1 h. The principal peak "a" results from P 1s → 3p transitions. For the HAp minerals, there exhibits a distinctive post-edge shoulder "b" and higher-energy peaks at around 2163 eV ("c") and 2170 eV ("d").[15, 31, 33] For the first 2 h, features b, c and d are less apparent, which are mixed with some amorphous $Ca_3(PO_4)_2$. While all of the features are similar to those of HAp after the CSH-IBU microspheres were soaked in the SBF solution for more than 3 h. The result of linear combination fitting at the P K-edge (Figure S3) is consistent with the Ca K-edge results (Table 3).

Table 3. P K-edge linear combination fitting results of samples after soaked in SBF solution in the first 3 hours.

	Percentage (%)		
	Amorphous CaP	HAp	R-factor
1 hour	22	78	0.006551
2 hour	6	94	0.005300
3 hour	1	99	0.004686

The observation at the Si K-edge is interesting (Figure 3C). During the IBU release process, there is only one prominent peak (labelled as "a") in the Si K-edge XANES spectra, which is identified as the Si 1s to 3p transition for silicon (IV) in a tetrahedral oxygen ligand environment.[31, 34] Comparing to the spectrum of the CSH-IBU before IBU release (0 h), the peak at lower photon energy labelled as "b", is due to the interaction between silanol groups (Si-OH) and carboxylic acid groups of IBU [27, 28] (less prominent in the FLY spectra, 0 h in Figure S4); it disappears nearly entirely in the spectra of CSH-IBU after IBU release. The disappearance of this peak once CSH-IBU microspheres were immersed in the SBF is likely due to the fast release of IBU from CSH carriers into SBF, resulting in the rapid decrease of the interaction between IBU and CSH. Compared to the standard sample SiO_2, the spectra of CSH-IBU microspheres after IBU release for different time periods are all identical to that of SiO_2, indicating that some mesoporous CSH microspheres have been hydrolyzed into SiO_2 during IBU release.[35, 36] Interestingly, the feature "b" can be detected again in the Si K-edge TEY spectra after 6 hours release although the intensities are much weaker than before (0 h spectrum). The IBU release profile of mesoporous CSH microspheres in SBF is shown in Figure 4. Initially, there was a burst release effect at the early stage; about 85 % IBU were released in the first hour, and 97-98 % of loaded IBU were released after 4 hours. This type of release profile is suitable for an acute infection or inflammation, when an immediate high dosage is needed for a short period of time. Hence, according to the IBU release profile, the reappearance of feature "b" at the Si K-edge after 6h can be ascribed to the re-adsorption of IBU on the surface of the release products (SiO_2), since the equilibrium of IBU release was reached during that period of time. Since no SiO_2 phase was observed from XRD, all the SiO_2 components detected from XANES are amorphous.

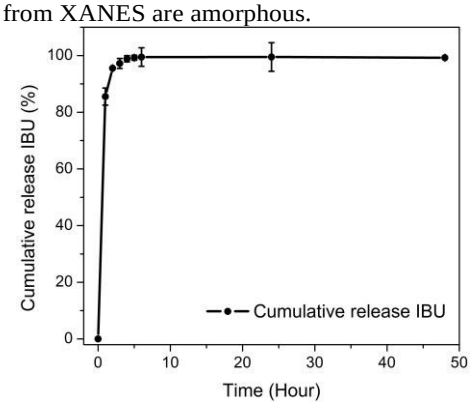

Fig. 4. The cumulative IBU release of mesoporous CSH microspheres in SBF.

Since it is shown that the CSH-IBU system starts to transform into crystalline HAp after having been soaked in the SBF solution for more than 4 h, it would be desirable if we could

identify and map the compositions of the *in vitro* samples after biomineralization at nanoscale. Figure 5A shows the STXM image of the CSH-IBU microspheres after having been soaked in the SBF solution for 5 h. No microspheres could be observed anymore; instead, an aggregation of flakes in several microns is seen. In order to monitor the components of the biomineralization product in details, we first obtain C K-edge XANES spectra isolated from 6 different regions of interest (ROIs) on the sample as shown in Figure 5B. All the ROIs were selected randomly based on the optical densities (sample thickness) to illustrate the uniformity/heterogeneity of various components at different edges. Since STXM is a powerful technique to study carbon nanomaterials and provides high quality absorption spectra with submicron spatial resolution,[37-39] C K-edge XANES from different ROIs could reveal the presence of residual IBU and carbon related compounds. From Figure 5C, compared with the spectrum of IBU powder (black profile), there is no significant change or beam damage to the residual IBU molecules on the drug release products: the sharp peak "a" located at 285 eV is from the carbon 1s to π* transition for the aryl rings of IBU molecules; the peak "b" located at 288.3 eV is from the carbon 1s to π* transition for carboxylic functional groups of IBU; the less apparent feature "c" became more prominent after having been soaked in SBF for 5h, and slightly shifted to higher photon energy, indicating the presence of carbonate ions.[40-44]

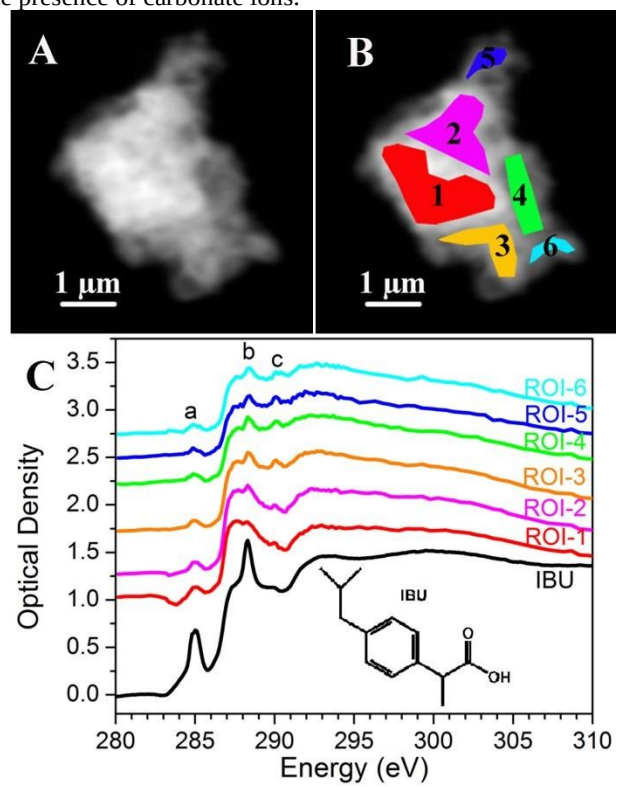

Fig. 5. (A) STXM optical density image of CSH-IBU sample soaked in SBF for 5h (averaged from 280 to 2190 eV); (B) ROIs taken from the CSH-IBU sample: Red: ROI-1, Magenta: ROI-2, Orange: ROI-3, Green: ROI-4, Blue: ROI-5 and Cyan: ROI-6; (C) XANES spectra taken from each ROI displayed in (B) at the C K-edge.

We have also compared the XANES spectra isolated from different ROIs at the Si K-edge (Figure 6C) and the P K-edge (Figure 6D); it is interesting to note that the strongest P signals were detected in ROI-1 and ROI-2 (red and magenta spectra of Figure 5D), where show the highest Si optical densities as well. Since STXM can determine the absolute thickness of the sample, SiO_2 and HAp thickness distributions are shown in Figure 6A and B, respectively.

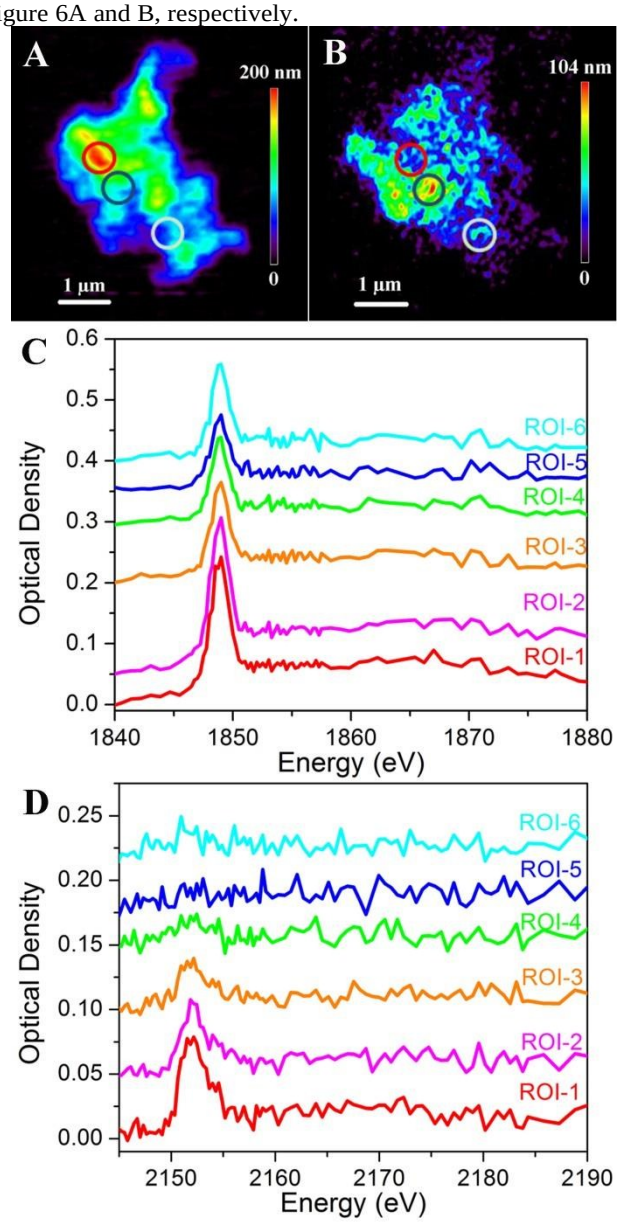

Fig. 6. Thickness distribution maps of CSH-IBU sample soaked in SBF for 5h at (A) the Si K-edge and (B) the P K-edge. The vertical bar illustrates the color code of the material thickness; XANES spectra of CSH-IBU sample soaked in SBF for 5h at the Si K-edge (C) and P K-edge (D) (ROI 1-6 are the same regions as shown in Figure 4B).

For STXM thickness modelling procedure, XANES spectra were obtained by converting the signal to optical density (OD) based on Beer-Lambert Law:

$$OD = -\ln(\frac{I}{I_0}) = \mu \cdot \rho \cdot t \quad (1)$$

where I_0 and I are the incident and transmitted X-ray photon flux (photons), respectively. μ is the energy dependent mass absorption coefficient (cm^2/g), ρ is the density (g/cm^3) of the material, and t is the sample thickness (nm). Then these spectra

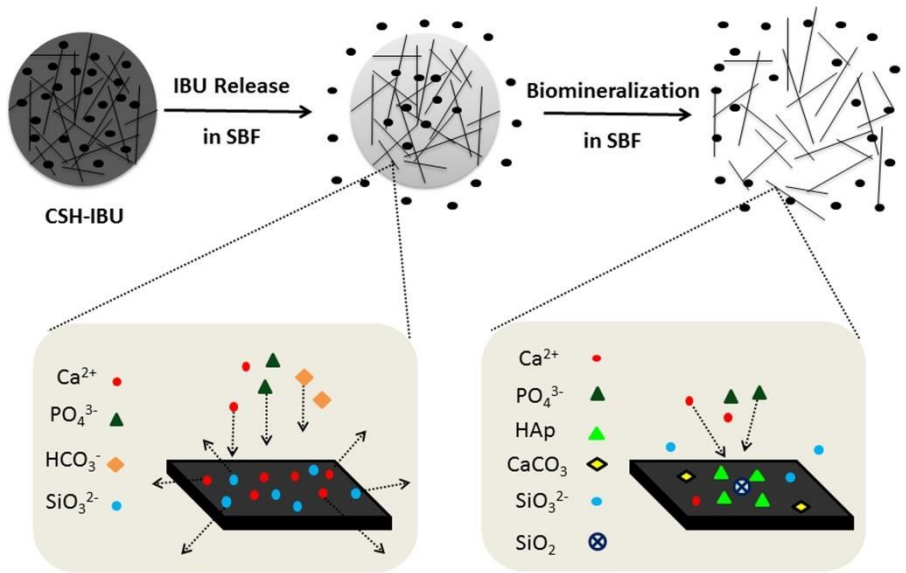

Fig. 8. Illustration of the proposed mechanisms for the IBU (black dots) release from mesoporous CSH microspheres and biomineralization.

were converted to absolute linear absorbance scales (optical density per nm thickness sample). The elemental linear X-ray absorption, which neglects interactions such as bonding among the atoms, is calculated by aXis2000 using equation (1) and (2):

$$\mu = \frac{N_A}{MM} \sum_i x_i \cdot \sigma_{ai} \qquad (2)$$

where N_A is the Avogadro's number, MM is the molecular weight of a compound containing x_i atoms of type i, σ_{ai} is the atomic photo absorption cross section (cm^2/atom) for type i atom. Then, the thickness was obtained by comparing the OD of each pixel in a STXM image and reference spectra. In this study, silicon and carbon reference spectra were obtained by fitting the original XANES spectra to match its calculated elemental linear X-ray absorption profile: hydroxyapatite ($Ca_5(PO_4)_3(OH)$: density = 3.160 g/cm^3, and thickness = 1 nm, silicon dioxide (SiO_2: density = 2.650 g/cm^3, and thickness = 1 nm) in the pre-edge and continuum. The thickness was obtained from stack fitting with the quantitatively scaled reference spectra of 1 nm thickness (Figure 7).

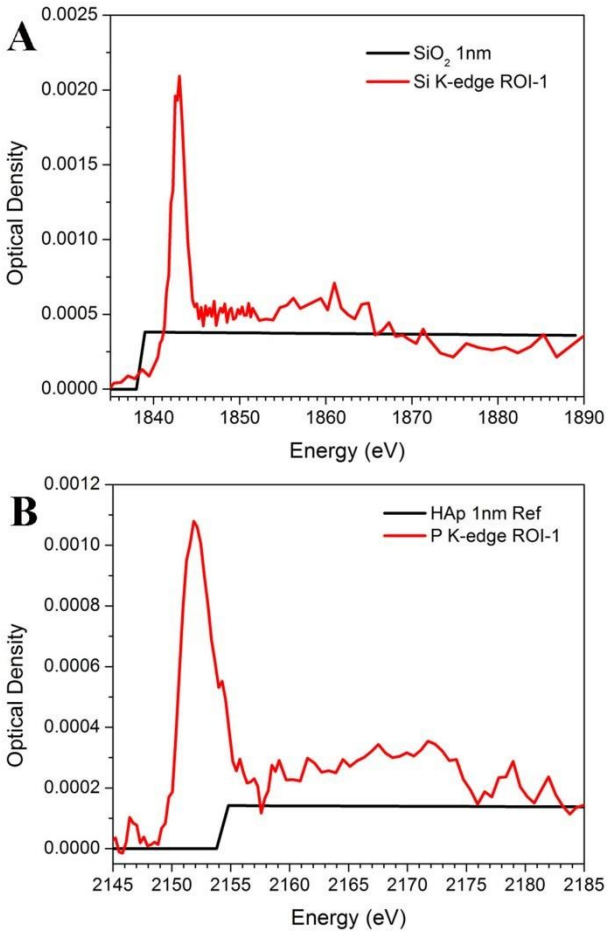

Fig. 7. Reference spectra and elemental linear X-ray absorption profiles of SiO_2 (a) (black profile: optical density spectrum of 1 nm thickness based on formula SiO_2; red profile: elemental linear X-ray absorption profile) and HAp (b) (black profile:

optical density spectrum of 1 nm thickness based on formula $Ca_5(PO_4)_3(OH)$; red profile: elemental linear X-ray absorption profile).

After 5 h *in vitro* test, most of the SiO_2 were located in the top left area with the largest thickness around 200 nm (± 10%). Moreover, one can see that from Figure 6B, more HAp can be detected around the red areas. The average SiO_2, HAp thickness of selected areas is given in Table 4 (the areas are shown in circles with different colors in Figure 6A and B).

Table 4. Thickness of SiO_2 and HAp in different regions.

	Average Thickness [nm]	
	SiO_2 Map	HAp Map
Circle 1 (Red)	173	36
Circle 2 (Navy)	91	86
Circle 3 (White)	73	27

There is ± 10% thickness deviation according to Figure 5

It is interesting to note that area 2 (navy circle) and 3 (white circle) have the similar thickness of SiO_2, however, the thicknesses of HAp in those areas are quite different. This is largely because area 2 is closer to area 1 (red circle) where most SiO_2 are located. During the biomineralization processes, some CSH microspheres (silanol abundant) [45-47] partially broke down and some silicate hydrolyzed into SiO_2 (area 1); this aggregation provides preferred further nucleation site for the growth of HAp. [10, 48, 49] That explains why we observe more HAp in area 2 rather than area 3.

Finally, based on all the above results, the processes of drug release and CSH biomineralization emerge. As illustrated in Figure 8, at the early stages of drug release, crystalline CSH microspheres disassemble into amorphous flake-like sheets, some silicate ions undergoes exchange into the SBF solution while others becomes hydrolyzed into amorphous silica. Both Ca (from CSH and SBF) and PO_4^{3-} ions (from SBF) first form amorphous calcium phosphate at first 2h, then quickly transformed into amorphous HAp (Figure S5), and the finally products were crystalline HAp after the samples were soaked in the SBF solution for more than 3h. At the same time, some bicarbonate ions (HCO_3^-) co-precipitate from SBF, generating amorphous $CaCO_3$. Moreover, from STXM data, more P were detected around the area where more Si were located; indicating the abundant silanol groups and the following hydrolyzed SiO_2 provided preference aggregation sites of HAp.

Conclusions

In this article we have illustrated that mesoporous CSH microspheres have very large drug loading capacities, which can reach as high as 1.80 g/g (Figure S6). The CSH-IBU system has a rapid drug release profile, which is suitable for acute disease (need of high drug dosage in a short period of time). The biomineralization mechanism for mesoporous CSH microspheres loaded with IBU in the SBF solution was elucidated via XANES and STXM. What's more important, we have demonstrated that synchrotron radiation is a very sensitive and powerful technique to study bioceramics: XANES has the ability to identify the chemical form of products (Si, P and Ca K-edge) even they are amorphous state. Using the highly-collimated STXM beam (best resolution: 30 nm), we provided spatial evidence of biomineralization formation (Si and P particularly).

Acknowledgements

The authors would like to acknowledge Dr. Richard B. Gardiner in Biotron of Western for his assistance in TEM measurement. The technical assistance from Mr. Chao Qi in Shanghai Institute of Ceramics is greatly acknowledged. We also thank Mr. Jun Li for the collection data at the Canadian Light Source. Research at the University of Western Ontario is supported by NSERC, CRC, CFI, OIT and ASPIRE. The Canadian Light Source is supported by CFI, NSERC, NRC, CHIR, and the University of Saskatchewan. Research at Shanghai Institute of Ceramics is supported by the National Natural Science Foundation of China (51172260, 51302294) and Science and Technology Commission of Shanghai (11nm0506600, 12ZR1452100).

Notes and references

[a] Department of Chemistry, University of Western Ontario, London, Ontario N6A 5B7, Canada.
[b] Shanghai Institute of Ceramics, Chinese Academy of Sciences, Shanghai 200050, China.
[c] Canadian Light Source, Saskatoon, Saskatchewan S7N 2V3, Canada.

† Electronic Supplementary Information (ESI) available: Morphologies of mesoporous CSH microspheres before and after IBU loading; details of linear combination fitting; Si K-edge FLY spectra of biomineralization of CSH-IBU; results of drug loading capacities test, results of IBU release from CSH microspheres in SBF solution; details of concentration change of Ca, Si, and P in SBF solution can be found in the supporting information. See DOI: 10.1039/b000000x/

1. D. Arcos and M. Vallet-Regi, *Acta Mater.*, 2013, 61, 890-911.
2. L. L. Hench, R. J. Splinter, W. C. Allen and T. K. Greenlee, *J. Biomed. Mater. Res.*, 1971, 5, 117-141.
3. P. Siriphannon, Y. Kameshima, A. Yasumori, K. Okada and S. Hayashi, *J. Eur. Ceram. Soc.*, 2002, 22, 511-520.
4. P. Siriphannon, Y. Kameshima, A. Yasumori, K. Okada and S. Hayashi, *J. Biomed. Mater. Res.*, 2002, 60, 175-185.
5. Z. Gou and J. Chang, *J. Eur. Ceram. Soc.*, 2004, 24, 93-99.
6. X. H. Wan, C. K. Chang, D. L. Mao, L. Jiang and M. Li, *Mat. Sci. Eng. C*, 2005, 25, 455-461.
7. L. H. Long, L. D. Chen, S. Q. Bai, J. Chang and K. L. Lin, *J. Eur. Ceram. Soc.*, 2006, 26, 1701-1706.
8. N. J. Coleman, J. W. Nicholson and K. Awosanya, *Cem. Concr. Res.*, 2007, 37, 1518-1523.
9. M. Gandolfi, P. Taddei, A. Tinti, E. De Stefano Dorigo, P. Rossi and C. Prati, *Clin. Oral Invest.*, 2010, 14, 659-668.
10. X. Li, J. Shi, Y. Zhu, W. Shen, H. Li, J. Liang and J. Gao, *J. Biomed. Mater. Res. B*, 2007, 83B, 431-439.
11. T. K. Sham, *Int .J. Nanotechnol.*, 2008, 5, 1194-1246.
12. Y. Takahashi, T. Miyoshi, S. Yabuki, Y. Inada and H. Shimizu, *Atmos. Environ.*, 2008, 42, 6535-6541.
13. S. J. Naftel, T. K. Sham, Y. M. Yiu and B. W. Yates, *J. Synchrotron Radiat.*, 2001, 8, 255-257.
14. M. E. Fleet and X. Y. Liu, *Am. Mineral.*, 2009, 94, 1235-1241.
15. E. D. Ingall, J. A. Brandes, J. M. Diaz, M. D. de Jonge, D. Paterson, I. McNulty, W. C. Elliott and P. Northrup, *J. Synchrotron Radiat.*, 2011, 18, 189-197.
16. L. Liu, S. Kim, J. Chan and T.-K. Sham, *MRS Online Proceedings Library*, 2011, 1352, 63-68.
17. Y. Tamenori, M. Morita and T. Nakamura, *J. Synchrotron Radiat.*, 2011, 18, 747-752.

18. T. Tyliszczak, A. L. D. Kilcoyne, J. A. Liddle, T. Warwick, A. P. Hitchcock, H. Ade and D. K. Shuh, *Micros. Microanal.*, 2004, 10, 1018-1019.
19. A. P. Hitchcock, J. J. Dynes, G. Johansson, J. Wang and G. Botton, *Micron*, 2008, 39, 311-319.
20. M. Sivakumar and K. Panduranga Rao, *Biomaterials*, 2002, 23, 3175-3181.
21. W. Xia and J. Chang, *J. Control. Release*, 2006, 110, 522-530.
22. W. Xia and J. Chang, *J. Non-Cryst. Solids*, 2008, 354, 1338-1341.
23. J. Wu, Y. J. Zhu, S. W. Cao and F. Chen, *Adv. Mater.*, 2010, 22, 749-753.
24. T. Kokubo, *J. Non-Cryst. Solids*, 1990, 120, 138-151.
25. Z. Wang, J. Wang, T.-K. Sham and S. Yang, *J. Phys. Chem. C*, 2012, 116, 10375-10381.
26. Z. Wang, J. Wang, T.-K. Sham and S. Yang, *Nanoscale*, 2014, 6, 9783-9790.
27. X. Guo, J. Wu, Y.-M. Yiu, Y. Hu, Y.-J. Zhu and T.-K. Sham, *Phys. Chem. Chem. Phys.*, 2013, 15, 15033-15040.
28. X. Guo, Z. Wang, J. Wu, J. Wang, Y.-J. Zhu and T.-K. Sham, *Nanoscale*, 2015, 7, 6767-6773.
29. T. Yamamoto, *X-Ray Spectrom.*, 2008, 37, 572-584.
30. D. Eichert, M. Salome, M. Banu, J. Susini and C. Rey, *Spectrochim. Acta B*, 2005, 60, 850-858.
31. H. Demirkiran, Y. Hu, L. Zuin, N. Appathurai and P. B. Aswath, *Mater. Sci.Eng. C*, 2011, 31, 134-143.
32. L. Cormier and D. R. Neuville, *Chem. Geol.*, 2004, 213, 103-113.
33. K. Güngör, A. Jürgensen and K. G. Karthikeyan, *J. Environ. Qual.*, 2007, 36, 1856-1863.
34. D. Li, G. M. Bancroft, M. Kasrai, M. E. Fleet, X. H. Feng, K. H. Tan and B. X. Yang, *Solid State Commun.*, 1993, 87, 613-617.
35. C. J. Brinker, *J. Non-Crystal. Solids*, 1988, 100, 31-50.
36. M. Motisuke, V. Santos, N. Bazanini and C. Bertran, *J. Mater. Sci. Mater. Med.*, 2014, 1-7.
37. J. Zhou, J. Wang, H. Liu, M. N. Banis, X. Sun and T.-K. Sham, *The J. Phys. Chem. Lett.*, 2010, 1, 1709-1713.
38. J. Zhou, J. Wang, H. Fang, C. Wu, J. N. Cutler and T. K. Sham, *Chem. Commun.*, 2010, 46, 2778-2780.
39. J. G. Zhou, J. Wang, C. L. Sun, J. M. Maley, R. Sammynaiken, T. K. Sham and W. F. Pong, *J. Mater. Chem.*, 2011, 21, 14622-14630.
40. A. Jokic, J. N. Cutler, E. Ponomarenko, G. van der Kamp and D. W. Anderson, *Geochim. Cosmochim. Acta*, 2003, 67, 2585-2597.
41. K. Benzerara, T. H. Yoon, T. Tyliszczak, B. Constantz, A. M. Spormann and G. E. Brown, *Geobiology*, 2004, 2, 249-259.
42. Y. Zubavichus, A. Shaporenko, M. Grunze and M. Zharnikov, *J. Phys. Chem. A*, 2005, 109, 6998-7000.
43. J. Ha, S. Chae, K. W. Chou, T. Tyliszczak and P. J. M. Monteiro, *J. Mater. Sci.*, 2012, 47, 976-989.
44. J. A. Brandes, S. Wirick and C. Jacobsen, *J. Synchrotron Radiat.*, 2010, 17, 676-682.
45. A. Nonat, *Cem. Concr. Res.*, 2004, 34, 1521-1528.
46. X. D. Cong and R. J. Kirkpatrick, *Adv. Cem. Based Mater.*, 1996, 3, 144-156.
47. J. J. Chen, J. J. Thomas, H. F. W. Taylor and H. M. Jennings, *Cem. Concr. Res.*, 2004, 34, 1499-1519.
48. Y. Tanizawa and T. Suzuki, *J. Chem. Soc. Faraday Trans.*, 1995, 91, 3499-3503.
49. P. Li, C. Ohtsuki, T. Kokubo, K. Nakanishi, N. Soga, T. Nakamura and T. Yamamuro, *J. Mater .Sci. Mater. Med.*, 1993, 4, 127-131.

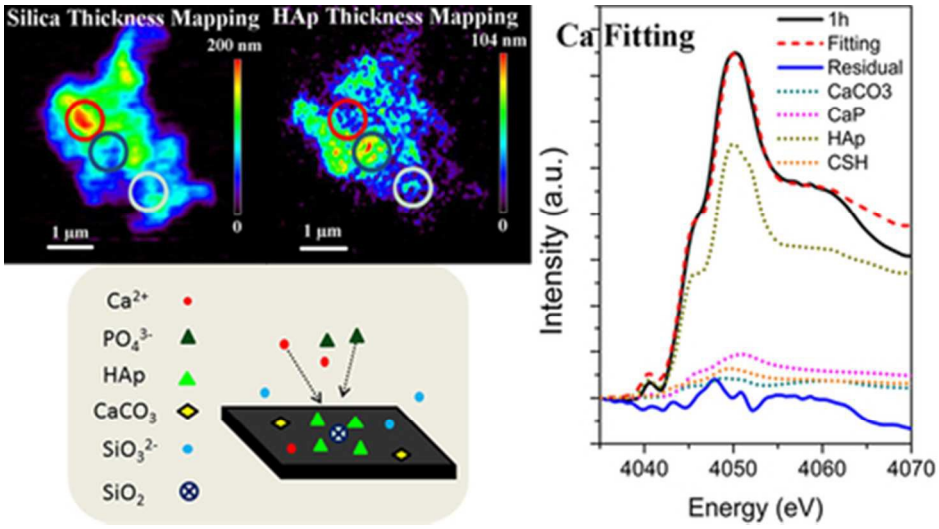

The imaging of silica indicated that they provided aggregation site of HAp, and amorphous CaCO3 were formed during CSH biomineraliztion.
39x21mm (300 x 300 DPI)